

# A hybrid classification-regression approach for 3D hand pose estimation using graph convolutional networks

Ikram Kourbane<sup>a,\*</sup>, Yakup Genc<sup>a</sup>

<sup>a</sup>*Gebze Technical University, Gebze, Kocaeli, 41000, Turkey*

## ARTICLE INFO

### Keywords:

3D hand pose estimation  
Graph convolutional networks  
Classification  
Multi-stage learning  
Monocular RGB image

## ABSTRACT

Hand pose estimation is a crucial part of a wide range of augmented reality and human-computer interaction applications. Predicting the 3D hand pose from a single RGB image is challenging due to occlusion and depth ambiguities. GCN-based (Graph Convolutional Networks) methods exploit the structural relationship similarity between graphs and hand joints to model kinematic dependencies between joints. These techniques use predefined or global learned joint relationships, which may fail to capture pose dependent constraints. To address this problem, we propose a two-stage GCN-based framework that learns per-pose relationship constraints. Specifically, the first phase quantizes the 2D/3D space to classify the joints into 2D/3D blocks based on their locality. This spatial dependency information guides this phase to estimate reliable 2D and 3D poses. The second stage further improves the 3D estimation through a GCN-based module that uses an adaptive nearest neighbor algorithm to determine joint relationships. Extensive experiments show that our multi-stage GCN approach yields an efficient model that produces accurate 2D/3D hand poses and outperforms the state-of-the-art on two public datasets.

## 1. Introduction


Hand pose estimation is one of the well-known and fast-growing topics in the computer vision community. It plays a significant role in multiple application domains, such as human-computer interaction, augmented reality, virtual reality and robotics. Although there is a large body of study in the literature, solving the 3D hand pose estimation problem remains challenging due to the similarity among fingers, self-occlusion and the complexity of the hand poses.

With the introduction of affordable commodity depth sensors and the rapid development of deep learning techniques, RGBD-based approaches achieve accurate 3D hand pose estimation results [1–7]. Other methods employ calibrated multi-view cameras to reduce the depth ambiguity [8, 9]. However, both depth and multi-view solutions are not readily available and work only in constrained environments. RGB-based methods are preferable since they are more accessible and do not require controlled settings. Due to the absence of depth information and occlusion, this task becomes an ill-posed problem. Furthermore, collecting 3D annotations for real images requires complex multi-view setups and manual annotations.

Learning-based methods tackle RGB-based 3D hand pose estimation by creating effective models trained on large-scale datasets [10–12]. We can divide them mainly into two categories. The first one adopts generative models to find the closest configuration (model-based) [10, 13–15]. The second category uses discriminative models to extract features and estimate the 3D pose (appearance-based) [16–21]. Despite the promising results, most of them assume that the model can implicitly learn kinematic relationships between the joints. However, this task is challenging and requires explicit constraints to guide the model optimization.

Inspired by the natural graph representation of the hand, recent studies use graph convolution networks (GCN) [22] to model skeletal constraints between joints [23–27]. [25] exploits annotated video frames to enforce spatial and temporal relationships between the joints based on predefined semantic meanings. This approach is limited to consecutive images, where temporal information is present. [26] estimates the 3D human pose by learning weighted relationships between body joints based on a predefined human skeletal. However, this approach misses potential relationships of physically disconnected joints. [27] addresses this limitation by replacing the skeletal relationships with global learnable constraints between all hand poses. But, different hand poses should not share the same relationship constraints since they do not have the same joint configurations (e.g: open and closed hands).

\*Corresponding author.

 [ikourbane@gtu.edu.tr](mailto:ikourbane@gtu.edu.tr) (I. Kourbane)

ORCID(s): 0000-0001-8753-6710 (I. Kourbane)

Motivated by these observations, we introduce a two-stage GCN-based framework to estimate 3D hand pose from a single RGB image. Unlike previous methods that either employ predefined joint relationship constraints [23, 25, 26] or learn a global one for the entire dataset [27], we learn per-pose relationship constraints expressing global and local joint spatial dependencies. Specifically, we propose a hybrid classification-regression framework that employs a light-weight feature extractor (ResNet-10) [28] and GCN modules [22] to classify each 2D/3D joint into its corresponding 2D/3D blocks based on its spatial locality. In particular, we divide our 2D/3D space into multiple classes such that neighboring joints belong to the same class. We utilize the classification probabilities to construct per-pose geometric constraints for 2D/3D joints. Afterward, we regress an initial (coarse) 3D hand pose using another GCN module that exploits learned constraints to guide the pose estimation task. (Fig. 1). Finally, we further improve the coarse pose using ANN-based (Adaptative Nearest Neighbors) GCN. Specifically, instead of fixing  $K$  neighbors for all the nodes (KNN), we calculate the distance between all joints to learn a differentiable threshold that determines the number of neighbors of each node in the graph. The proposed approach speeds up the running time since it includes lightweight feature extractor [28] and GCN-based modules [22]. The latter proved to be computationally efficient than CNNs [27]. We summarize our contributions as follows:

- We propose a two-stage GCN-based approach that combines classification and regression to estimate an accurate 3D hand pose from a single RGB image. The classifiers find spatial dependencies between neighboring joints to learn per-pose relationship constraints that guide the regression.
- Instead of KNN-based GCN, we propose an adaptative nearest neighbor algorithm that learns a different number of joint relationships improving the 3D hand pose estimation task.
- To evaluate our approach, we conduct extensive experiments on synthetic and real-world datasets. The reported quantitative and qualitative results demonstrate that our efficient method outperforms state-of-the-art and estimate accurate 2D/3D hand poses.

The rest of this paper is organized as follows: Section. 2 reviews the related studies of our work. Section. 3 explains the proposed method in-depth and describes the most important modules of our framework. Section. 4 presents experimental results on two public datasets and compares the proposed approach against the state-of-the-art. Finally, Section. 5 presents the conclusion of the study and direction for future work.

## 2. Related works

We classify 3D hand pose estimation methods based on the input modality into three categories depth-based, multi-view RGB-based, and monocular RGB-based. In the past few years, numerous studies adopt deep learning techniques to handle various types of inputs for depth methods, such as 2D pixels [1, 2, 4, 5], a set of 3D points [3, 6] or voxels [7]. In the second category, several studies use many RGB cameras on different angles to alleviate the occlusion problem [8, 9].

RGB cameras are more available compared to the two-mentioned categories. There are several attempts to solve the problem with model-based methods [29–31]. These methods search the closest configuration that fits the hand model via an optimization process. They require powerful prior knowledge about many dynamic and physics hypotheses, which leads to poor performances. Deep generative-based approaches exhibit promising performances and generate accurate 3D poses. [10] employs generative adversarial networks (GANs) [32] to translate synthetic labeled data to realistic images to reduce the domain gap. [13] uses Variational Autoencoders (VAEs) [33] to learn a shared latent space across RGB and depth modalities to remedy the missing depth ambiguity. However, These methods model black-box latent representations, which synthesize a single 3D pose for a given RGB image. To address this issue, [14, 15] disentangle the diverse factors that affect the hand visualization, including camera viewpoint, scene context and background.

Discriminative methods act as a function that maps directly between the RGB image and the 3D pose using large-scale annotated datasets. [17] is one of the first attempts that estimates the 3D hand pose from a monocular RGB image. It employs synthetic data and three concatenated networks: hand segmenter, 2D keypoint and 3D hand pose predictors. After this work, many deep-based studies have been proposed to improve 3D hand pose estimation. [16] estimates 3D hand poses by combining CNN with a kinematic 3D hand model. [18] leverage depth information to supervise the training by having a pair of RGB-RGBD images. [19] uses a two-stack hourglass with latent 2.5D heatmaps and lift

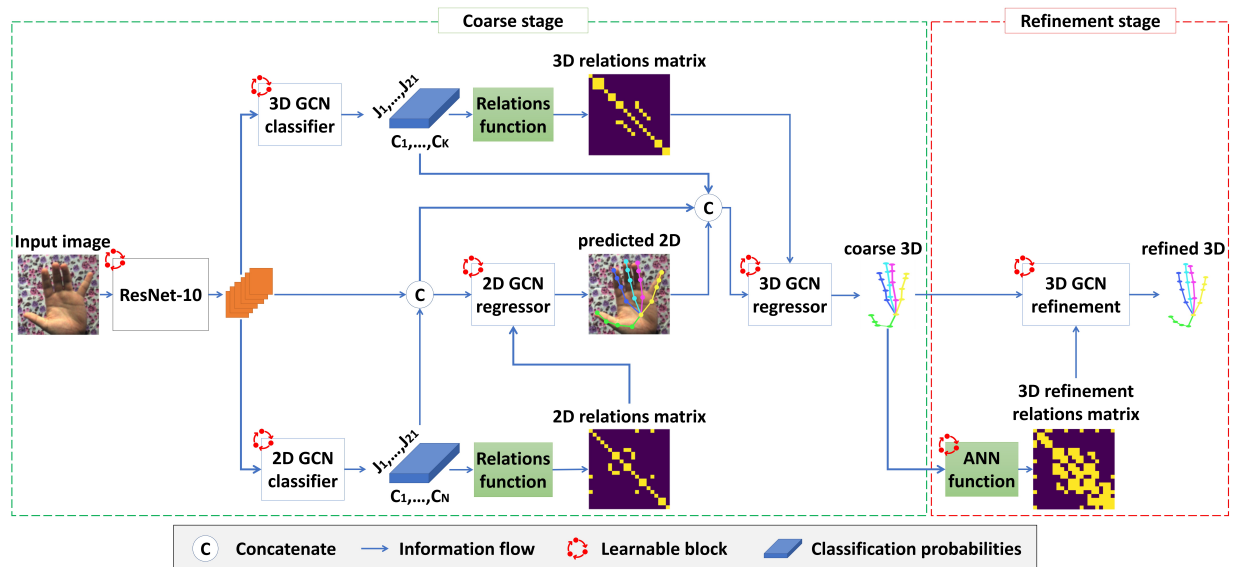


**Figure 1:** Schematic overview of our 3D pose estimation framework, where the input is the RGB hand image, and the output is the 3D pose. We extract image feature maps using a lightweight ResNet-10 network. We classify joints (i.e.,  $J_i$ ) in 2D and 3D spaces based on their spatial alignment such that neighboring joints belong to the same class  $C_i$ , where  $N$  and  $K$  are the number of classes in 2D and 3D spaces, respectively. We construct 2D/3D per-pose joint relationship constraints using 2D/3D GCN-based classifiers and *Relations* function. This knowledge guides 2D/3D GCN-based regressors to estimate reliable 2D/3D poses. We further improve the 3D pose using the refinement network that employs an adaptive nearest neighbors (ANN) function to identify joint relationships (This figure should be printed in color).

them to 3D. Other approaches achieve reliable 3D poses by regressing the hand mesh and estimating the 3D pose from it [20, 21, 34, 35]. However, these methods require additional supervision since the datasets must include both the meshes and the 3D poses. More recently, [36] proposed a knowledge distillation and generalization framework for RGB-based pose estimation.

GCN [22] became a hot topic of research in the computer vision field since there exist several problems that have graph-like structures as input. [23] applies GCNs [22] to estimate the 3D pose with the help of a weakly-supervised training strategy that employs depth regularizer. [25] exploits spatial and temporal relationships for 3D human and hand pose estimation tasks. [24] introduces a self-supervised module that uses 2D relationships and 3D geometric knowledge to reduce the gap between 2D and 3D spaces. [27] proposes a UNet-based GCNs to estimate the 3D hand pose and the 6D object pose. It learns global geometric relationship constraints for all hand poses. This paper introduces a GCN-based framework for 3D hand pose estimation using a single RGB image. It exploits the spatial dependencies information between joints to learn per-pose relationship constraints yielding better performance than the global one. The proposed approach does not require depth nor meshes supervision.

### 3. Methodology

Due to the absence of depth information, it is challenging to estimate accurate 3D hand poses from a monocular RGB image. We observe that one of the main obstacles for learning-based 3D hand pose estimation approaches is the non-exploitation of spatial dependencies between adjacent joints to constrain the 3D pose estimation task and reduce the depth ambiguity. Furthermore, [25, 27] show that coarse-to-fine techniques improve the 3D pose estimation accuracy. Motivated by these observations, we introduce an effective approach for 3D hand pose estimation from a monocular RGB image (Fig. 1).

Our approach is based on GCNs (Section. 3.1) and includes six main modules. A modified ResNet-10 described in Section. 3.2. 2D and 3D joint classifiers presented in Section. 3.3. Section. 3.4 explains the relations algorithm that constructs per-pose geometric constraints. This knowledge is combined with a global learnable constraint to regress 2D/3D hand pose (Section. 3.5). Section. 3.6 shows our proposed refinement network that employs the ANN algorithm to identify joint relationships improving the estimated pose. Finally, Section. 3.7 presents the loss functions. Note that

**Table 1**

The architecture of the modified ResNet-10 network

Layer	In	Out	Kernel	Stride	Padding
Conv2D	3	32	$7 \times 7$	2	3
BN	32	32	-	-	-
ReLU	32	32	-	-	-
Max-pool	32	32	3	2	1
Res-Block	32	32	$3 \times 3$	1	1
Res-Block	32	64	$3 \times 3$	2	1
Conv2D	32	64	$1 \times 1$	2	0
BN	64	64	-	-	-
Res-Block	64	128	$3 \times 3$	2	1
Conv2D	64	128	$1 \times 1$	2	0
BN	128	128	-	-	-
Res-Block	128	256	$3 \times 3$	2	1
Conv2D	128	256	$1 \times 1$	2	0
BN	256	256	-	-	-
Conv2D	256	21	$3 \times 3$	1	1

the architecture of our last five modules is based on GCNs, which are more efficient than CNNs [27].

### 3.1. Revisiting graph convolution network

GCNs are introduced in [22] to perform semi-supervised classification on graph-structured data. Unlike CNNs that can only handle fixed structures, GCNs treat irregular structures in a non-euclidian space. Let  $G = (V, E)$  denote a graph, where  $V$  and  $E$  represent a set of  $M$  nodes and  $L$  edges, respectively. Let  $A \in [0, 1]^{M \times M}$  be the adjacency matrix of  $G$ . Let  $I$  be the identity matrix and  $\tilde{A} = A + I$  is the new self-loop adjacency matrix. Since the graph may include low/high-degree nodes a normalization process is required to avoid vanishing/exploding gradients. [22] addressed this problem by scaling rows and columns of  $\tilde{A}$  in Eq. 1.

$$\hat{A} = \tilde{D}^{-\frac{1}{2}} \tilde{A} \tilde{D}^{-\frac{1}{2}} \quad (1)$$

Where  $\tilde{D}$  is the degree matrix of  $\tilde{A}$ . GCNs propagate information between nodes to update their representations. The adjacency matrix serves as a mask to select the aggregated nodes. The propagation rule in GCN is computed in Eq. 2:

$$H^{k+1} = \delta(\hat{A}H^k W^k) \quad (2)$$

Where:  $\delta = ReLU$  is the activation function,  $H^k$  and  $W^k$  are the node features and the weights in the  $k^{th}$  layer, respectively.

### 3.2. Feature maps extraction

We use a modified ResNet-10 architecture [28] as a backbone for feature extraction from an RGB hand image. We reduce the number of feature maps in each convolution layer (width) to improve efficiency without affecting the performances. We describe the details of our architecture in Table. 1. We feed the cropped hand into the network, and we flatten the last two dimensions of the feature maps from  $(B, 21, W, H)$  to  $(B, 21, W \times H)$ , where  $B$  is the batch size,  $W$  and  $H$  are the width and the height of the feature maps, respectively. The reason for this transformation is to get the correct input format for the 2D/3D GCN classifiers, where each joint has a feature vector of size  $W \times H$ .

### 3.3. Classification modules

We feed the output feature maps of the ResNet-10 network to 2D/3D GCN-based classifiers [22] to assign each 2D/3D joint to a specific 2D/3D block, respectively, based on its locality. This task is less challenging than regression since the output dimension is restricted. Furthermore, it exploits spatial dependencies between the joints (nodes) to learn 2D/3D per-pose relationship constraints that serve as additional information during pose estimation.

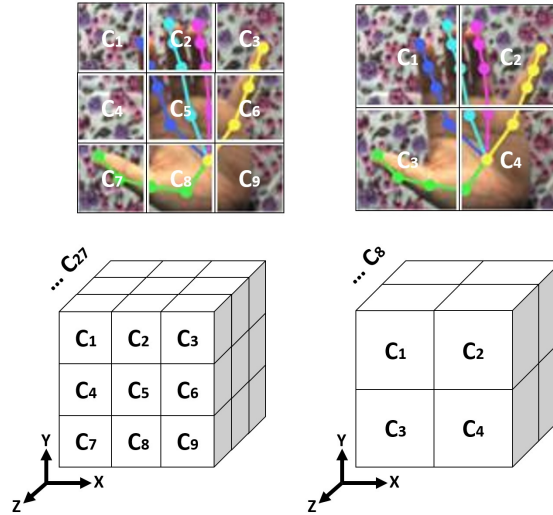


**Figure 2:** We classify each joint position into a predefined number of classes by dividing the 2D and 3D space into discrete intervals in the  $[X, Y]$  and  $[X, Y, Z]$  axes, respectively. The top and the bottom rows demonstrate two examples of 2D and 3D quantization. Due to visualization difficulties, we represent the 3D classes by cubes (This figure should be printed in color).

To train our classifiers, we need the ground truth classes for 2D and 3D joints. Following Algorithm. 3, we classify each 2D joint into one of the 2D blocks based on its  $(x, y)$  coordinates. Specifically, we divide the 2D space into  $N = n \times n$  blocks where  $n$  is the number of splits in the horizontal and the vertical axis of the image. The shape of 2D classes is  $(B, N, 21)$ , where  $B$  is the batch size and 21 is the number of joints. Fig. 2 illustrates the quantization process of the joints in 2D and 3D spaces.

In the 3D joint classification, we divide the 3D space into  $K = k \times k \times k$  blocks where  $k$  is the number of splits in the  $x, y$  and  $z$  axis. Following Algorithm. 4, we classify each 3D joint into one of these 3D blocks based on its  $(x, y, z)$  coordinates. The shape of 3D classes is  $(B, K, 21)$  and the output of the 2D/3D classifier in Fig. 1 is a tensor of class probabilities for each joint.

In this stage, we use the propagation rule in [27] to classify 2D/3D joints. Specifically, our GCNs learn global adjacency matrix  $\hat{A}$  (constraints) instead of feeding a predefined one [22]. We empirically set the number of graph convolution layers of our network to two, where each layer is defined in Eq. 2. We feed the estimated values to the *Relations* function in Algorithm. 1, which outputs a per-pose 2D/3D geometric relationship constraints to guide the pose estimation task. In particular, 2D/3D per-pose adjacency matrix expresses spatial dependencies between each pair of joints. We find that the GCN-based classifier exhibits better performance than Fully Connected (FC) networks. Note that we quantized the 2D/3D interval into overlapped blocks to consider the problem of joints residing in borders. However, we do not notice any gain over the proposed classification approach. We can explain this by that using overlapped blocks increases the number of classes reducing accuracy performances. Also, a joint can belong to different classes, which confuses the classifier.

### 3.4. Relations function

We employ the *Relations Function* described in Algorithm. 1 to express geometric constraints between the joints. It constructs a 2D/3D per-pose adjacency matrix that serves as an extra weighting for the GC layers. The algorithm takes the output of the 2D/3D classifier, applies a *Softmax* activation function to get class probabilities of each joint and an *Argmax* function to find the class corresponding to the highest probability. Finally, adjacent joints are identified by comparing their labels. The output matrix is of size  $21 \times 21$  where each  $(i, j)$  coordinate exhibits the relation between  $joint_i$  and  $joint_j$ . Note that the proposed function can identify relations between pairs, which are physically disconnected in the hand skeletal model.

---

**Algorithm 1:** Relations function.

---

```

1 function RelationsFunction (data);
   Input : Classifier outputs for each joint.
   Output: 21 × 21 relations matrix.
2 matrix ← [];
3 probabilities ← softmax(data, dim = 1);
4 labels ← argmax(probabilities, dim = 1);
5 for i=0:21 do
6     values ← [];
7     for j=0:21 do
8         a ← labels[:, i];
9         b ← labels[:, j];
10        values[j] ← (a == b);
11    end
12    matrix[i] ← values;
13 end
14 return matrix;
```

---

### 3.5. Regression modules

This module aims to estimate 21 2D/3D hand joints from a monocular RGB image. [27] estimates the 3D poses using Eq. 2 as a propagation rule. It learns a global adjacency matrix between all the poses in the dataset. Although [27] outperforms the limitation of [23, 25] that do not include relations of physically disconnected joints, it presents another problem. In particular, learning only a global adjacency matrix is a potential limitation since different hand poses in the dataset share a single relationship constraint (e.g. open and close hands have the same adjacency matrix despite being physically dissimilar). Our 2D/3D GCN-based regressors exploits the estimated 2D/3D per-pose adjacency matrices  $R_{2D}$  and  $R_{3D}$  as local constraints for each hand pose (Eq. 3 and Eq. 5). Besides, It keeps the learnable adjacency matrix  $\hat{A}$  [27] that expresses global relationships. This combination guides the 2D/3D hand pose regressors to provide an initial promising pose using Eq. 4 and Eq. 6.

$$R_{2D} = RelationsFunction(L_{2D}) \quad (3)$$

$$H_{2D}^{k+1} = ReLU([\hat{A}H_{2D}^k W_A^k, R_{2D}H_{2D}^k W_R^k]) \quad (4)$$

Where:  $L_{2D}$  is the output of the 2D classifier,  $H_{2D}^0$  is the concatenation of the ResNet-10 features and the 2D classifier probabilities.  $W_A^k$  and  $W_R^k$  are the weights for the global and the local adjacency matrices, respectively.

Recent works demonstrate that 2D pose information improves the 3D pose estimation task [26, 37, 38]. We feed the concatenation of the estimated 2D poses, the image feature maps of the ResNet-10 network, the 2D classification probabilities and the 3D classification probabilities ( $H_{3D}^0$ ) to the 3D regressor. Furthermore, we exploit the 3D relations matrix (Eq. 5) as an additional weighting mechanism during neighborhood aggregation to express the spatial dependencies between the 3D joints (Eq. 6).

$$R_{3D} = RelationsFunction(L_{3D}) \quad (5)$$

$$H_{3D}^{k+1} = ReLU([\hat{A}H_{3D}^k W_A^k, R_{3D}H_{3D}^k W_R^k]) \quad (6)$$

Where:  $L_{3D}$  is the output of the 3D classifier.

### 3.6. 3D refinement module

After getting reliable 2D/3D poses from the coarse stage, we freeze the network weights, and we improve the estimated 3D pose through a refinement module. The latter applies the proposed ANN algorithm to construct a per-pose adjacency matrix for the GCN. Previous works employ KNN-based graphs for other computer vision tasks. [39, 40] create graphs from image features and apply residual KNN-based GCN for face clustering. [41] connects KNN 3D



points cloud for RGBD semantic segmentation. However, fixing a unique number of nearest neighbors  $K$  for all the hand poses of the dataset does not capture the underlying structure of joints, which may affect information aggregation in the GCN. Moreover, the same hand pose may include high-degree nodes (joints) as well as low-degree ones. Hence, the number of nearest neighbors should be different for each joint based on its distance to the others.

To alleviate this problem, we first calculate the distance matrix  $D \in R^{21 \times 21}$  among 21 joints. Subsequently, we learn a global threshold  $T$  to be the criteria to select the related joints. Following Algorithm. 2, if  $D(i, j) \leq T$  then joint  $i$  and joint  $j$  are considered as adjacent and  $R_{ANN}(i, j) = 1$ , where  $R_{ANN}$  is the adjacency matrix. We feed  $R_{ANN}$  and the prior estimated pose  $H_{3D}^0$  to GCN refinement to produce a more accurate pose (Eq. 7). Note that the gain of the adaptative ANN-based GCN module appears when the coarse pose is predicted from our hybrid classification-regression approach. In other words, estimating 3D poses without using the proposed local constraints (2D/3D per-pose adjacency matrix) produces less accurate coarse poses. Thus, ANN may identify wrong nearest neighbors in the adjacency matrix.

$$H_{3D}^{k+1} = ReLU([\hat{A}H_{3D}^k W_A^k, R_{ANN}H_{3D}^k W_R^k]) \quad (7)$$

---

**Algorithm 2:** Adaptative nearest neighbour algorithm.

---

```

1 function ANN(3D, θ);
   Input  : 3D: coarse predictions, θ: learnable threshold
   Output: 21 × 21 ANN relations matrix.
2 matrix ← [];
3 for i=0:21 do
4     values ← [];
5     for j=0:21 do
6         | values[j] ← MSE(3D[i], 3D[j]);
7     end
8     matrix[i] ← values;
9 end
10 matrix = float(matrix <= θ);
11 return matrix;
```

---

### 3.7. Loss functions

Our training schema is composed of two stages coarse and refinement. The former involves two loss terms for the classification and the regression. Eq. 8 and Eq. 9 classify each joint into one of the blocks in the 2D/3D space, where  $CE(\cdot)$  is a multi-class Cross-entropy loss function. In Eq. 10 and Eq. 11, we use an  $L_2$  regression loss between the predicted and the ground truth 2D/3D joints.

$$L_{classification2d} = \sum_{i=1}^{21} CE_i(PredictedClass2D_i, GTClass2D_i) \quad (8)$$

$$L_{classification3d} = \sum_{i=1}^{21} CE_i(PredictedClass3D_i, GTClass3D_i) \quad (9)$$

$$L_{regression2d} = L_2(Predicted2DPose, GT2DPose) \quad (10)$$

$$L_{regression3d} = L_2(Predicted3DPose, GT3DPose) \quad (11)$$

The coarse loss in Eq. 12 is a linear combination of the regression and the classification loss, where  $\delta_1 = 100$  and  $\delta_2 = 1$  for the regression and the classification terms, respectively. We empirically find the best hyperparameters by trying different configurations.

$$L_{coarse} = \delta_1 * (L_{regression2d} + L_{regression3d}) + \delta_2 * (L_{classification2d} + L_{classification3d}) \quad (12)$$

In the refinement stage, we use the  $L_2$  loss between the ground truth 3D and the predicted one (Eq.13).

$$L_{refinement} = L_2(Fine3DPose, GT3DPose) \quad (13)$$

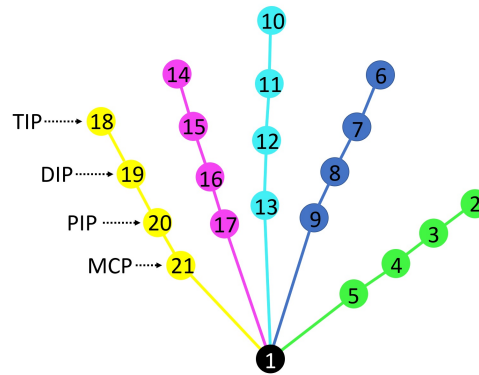


**Figure 3:** The description of our hand model, where the first joint is the wrist. For each finger from the thumb to the pinky, the order starts from the tip to the mcp (This figure should be printed in color).

## 4. Experiments

### 4.1. Implementation details

We implement the proposed method using Pytorch v1.6 [42], CUDA v10.1 and cuDNN v7.6.4. We train our model on images of size  $256 \times 256$  for 400 epochs using a batch size of 64. We initialize the weights of the ResNet-10 network using a normal distribution, where the  $mean = 0$  and  $std = 0.02$ . We initialize the weights of the GCN networks using Xavier [43] where we set the gain to the square root of 2. We use NVIDIA’s Apex mixed-precision training of 16-bits to speed-up the training. It takes three days to converge on a single NVIDIA TITAN X GPU. We empirically found that AdaDelta optimizer [44] is better than ADAM [45] for our task. Since the weights updating formula does not include a learning rate, we use the default optimizer parameters.

### 4.2. Datasets and evaluation metrics

To train and evaluate our proposed method, we need datasets that include RGB images with their 2D and 3D annotations. We conduct our experiments using the Stereo Hand Pose Tracking Benchmark (STB) [46] [dataset] and Rendered Hand Pose (RHD) [dataset] datasets [17]. These benchmarks are widely used for 3D hand pose estimation from a monocular RGB image.

STB [46] contains 30k and 6K real-world images for training and test, respectively. This dataset provides the RGB images with their corresponding 3D annotations. To obtain the 2D keypoints, we perform a projection operation from the 3D space using the given camera intrinsic parameters. This dataset is less challenging since it has less lighting, viewpoint, and background variations. Also, the images are not noisy and have high resolution ( $640 \times 480$ ).

RHD [17] is a very challenging hand dataset that contains synthetic images of resolution  $320 \times 320$  collected from twenty persons performing 39 actions. The images are rendered from several viewpoints and using different illumination conditions. RHD dataset contains 41K images for training and 3K images for testing covering several backgrounds and hand shapes. Each sample in the dataset includes an RGB image, a hand mask image, the corresponding depth image, the 2D key-points and the 3D hand pose.

To crop the hand from the image, we find the  $min_x$ ,  $min_y$ ,  $max_x$  and  $max_y$  of the 2D points. The top left corner ( $min_x, min_y$ ) and the bottom right corner ( $max_x, max_y$ ) are subtracted/added to a small threshold of 10 and 20 for the RHD and STB datasets, respectively, ensuring that the cropped hand image includes all the joints.

To evaluate our approach and quantitatively compare it against the state-of-the-art methods, we report the common metric mean end-point-error (EPE), which measures the average Euclidean distance between the ground-truth and the estimated keypoint. The distances are expressed in millimeters (mm) and pixels (px) for 2D and 3D hand pose estimation, respectively. Furthermore, we show the area under the curve (AUC) on the percentage of correct keypoints (PCK), which is widely used to evaluate human/hand pose estimation approaches with different thresholds. Although the main aim of the proposed method is to estimate the 3D hand pose, we also validate the classification performance using common metrics, including accuracy, precision and recall.



**Table 2**

Ablation studies of different baselines with mean EPE [mm] and AUC on the RHD dataset (for EPE lower is better, for AUC higher is better).

Method	$EPE^-$	$AUC^+$
Baseline A: full w/o classification	19.16	0.858
Baseline B: full w/o refinement (coarse)	14.76	0.927
Baseline C: full w/ FC refinement	14.68	0.928
Baseline D: full w/ KNN refinement	13.43	0.935
Full	<b>12.81</b>	<b>0.939</b>

### 4.3. Hand model representation

We follow the hand model of [17, 46] (Fig. 3), such that the hand is described by 21 joints, namely the wrist representing the hand palm and four joints (tip, dip, pip and mcp) per finger (thumb, index, middle, ring and pinky). Since we aim to identify the spatial relationships between each pair of joints in 2D/3D space, the order of the joints and fingers is important to understand the proposed per-pose constraints (adjacency matrices). We define each joint position by  $joint_{2D} = (x, y)$  and  $joint_{3D} = (x, y, z)$  for 2D and 3D coordinates, respectively.

### 4.4. Self-comparisons

To evaluate the proposed approach and find the best design choice, we conduct extensive experiments on the RHD dataset since it is more challenging. We first investigate the impact of our hybrid classification-regression approach (per-pose constraints) on the hand pose estimation performances. We analyze the effect of the number of classes, and we show the benefit of the proposed ANN-based refinement module. We select the best model to run it on the STB dataset and compare it against the state-of-the-art methods.

#### 4.4.1. Analysis of the classification modules (per-pose constraints)

To validate the proposed hybrid classification-regression method, we perform two different experiments. The first one is *Baseline A* that employs ResNet-10 and 2D/3D GCN-based regressors without the refinement module. Furthermore, it uses only the global learned relationship constraints (adjacency matrix) to estimate the 2D/3D hand pose, respectively. In particular, we remove the classification modules that provide 2D/3D per-pose constraints from the framework in Fig. 1. In the second experiment, we implement the proposed approach (*Full*) that classifies the joints into several 2D/3D blocks to find a spatial relationship between the joints. We employ this information as an individual adjacency matrix for each sample of the dataset (per-pose constraint) to estimate promising coarse poses. In the second stage, the ANN-based GCN refines the initial 3D pose to generate a more accurate one. We can see from Table. 2 that our proposed method (*Full*) outperforms *Baseline A* that provides lower scores in both AUC and EPE metrics proving the superiority of the proposed per-pose constraint over the global shared one.

#### 4.4.2. Effect of the number of classes

We conduct a set of experiments to find the best number of 2D/3D blocks (classes) that provide the best performances. We compare the effect of 4, 9, 16 and 25 classes by dividing the 2D space into  $(2 \times 2)$ ,  $(3 \times 3)$ ,  $(4 \times 4)$  and  $(5 \times 5)$  blocks, respectively. Besides, we compare the effect of 8, 27, 64 and 125 classes by dividing the 3D space into  $(2 \times 2 \times 2)$ ,  $(3 \times 3 \times 3)$ ,  $(4 \times 4 \times 4)$  and  $(5 \times 5 \times 5)$  blocks, respectively. Table. 3 shows that our GCN-based classifiers yield high performance if the number of classes is less than 27. We note that having a large number of classes produces an identity-like adjacency matrix. Meanwhile, having a small number of classes increases the adjacent joints, and the matrix will not effectively express relations. We empirically fix the best number of classes to 16 and 27 for the 2D and 3D classifiers, respectively. This configuration achieves high classification performances and constructs meaningful per-pose relation matrices improving the 2D/3D pose estimation.

#### 4.4.3. Effect of the refinement network

As mentioned previously, our approach estimates an initial 3D hand pose in the coarse stage. In the second stage, the refinement network takes as inputs the estimated coarse pose and the learned ANN adjacency matrix to obtain a more accurate pose. To investigate the impact of this module, we report the quantitative results of the coarse prediction (*Baseline B*) in Table. 2. Also, Fig. 4 shows the qualitative results of the coarse estimation, the refined estimation and

**Table 3**

Effect of the number of classes on our 2D/3D classifiers. Each triplet in the classification metrics represents the accuracy, recall and precision.

2D classes	2D classification metrics	3D classes	3D classification metrics
4	99.98/99.94/99.88	8	99.97/99.92/99.82
9	99.96/99.90/99.81	27	99.83/99.78/99.71
16	99.91/99.87/99.78	64	95.15/94.92/94.53
25	99.86/99.82/99.73	125	88.11/86.74/85.23

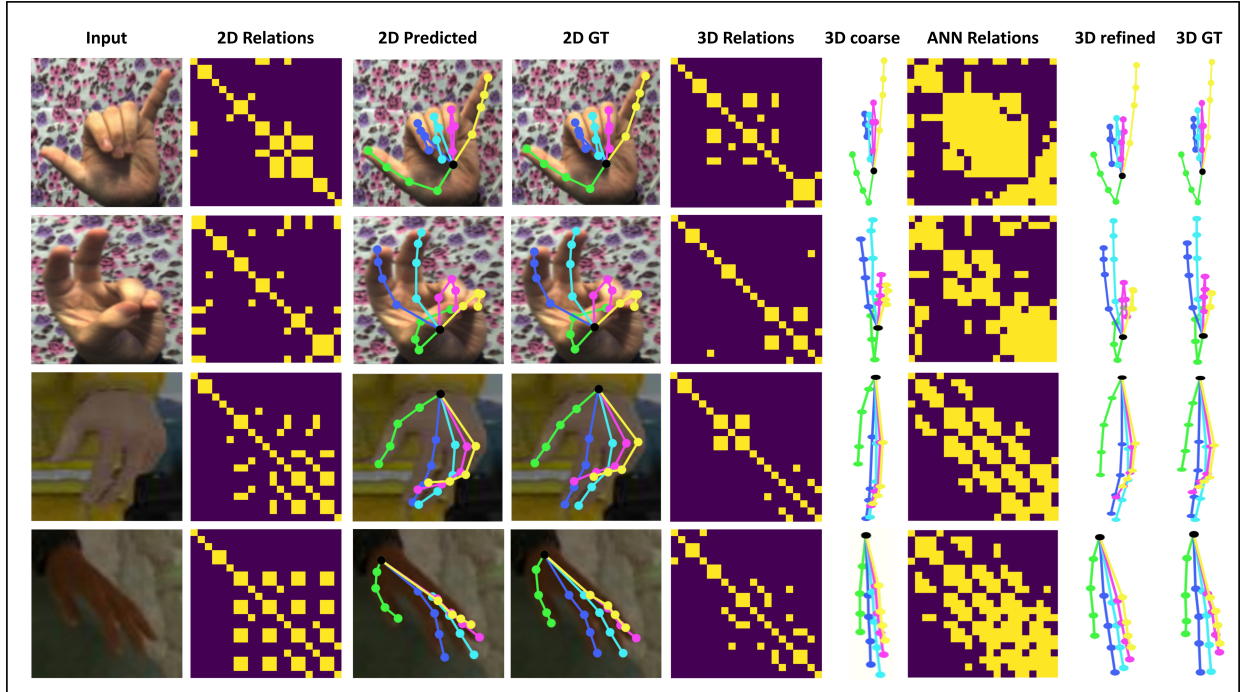


**Figure 4:** The intermediate output of the proposed method on STB and RHD datasets. From left to right, we show the input hand image, the per-pose 2D relations matrix, the predicted 2D key-points, the ground truth 2D keypoints, the per-pose 3D relations matrix, the predicted coarse 3D pose, the per-pose ANN relations matrix, the refined 3D pose and the ground truth 3D pose (This figure should be printed in color).

the learned per-pose adjacency matrices. We can see that the refinement module improves the coarse prediction and achieves more reliable qualitative and quantitative results. We can explain this by that the proposed ANN technique uses the estimated coarse 3D poses to provide a precise per-pose adjacency matrix. Hence, exploiting this information at this stage yields more accurate spatial dependencies and improves performance. Table. 2 shows a significant margin between the full model and *Baseline A*. The latter estimates the coarse pose without exploiting per-pose constraints to identify spatial relations. Therefore, applying the proposed ANN on *Baseline A* identifies wrong related joints and lead to poor performance.

The GCN-based refinement modules outperform the simple FC refinement module (*Baseline C*) demonstrating the superiority of GCN to fit the problem of hand pose estimation. To validate the proposed ANN algorithm, we compare it against KNN (*Baseline D*), where we empirically fix  $K$  to 5. Results show that the ANN-based refinement module outperforms the KNN-based version (Table. 2). We can explain this by that the KNN adjacency matrix learns the same number of adjacent joints regardless of the pose and the joint locations. On the other hand, we can see from (Fig. 4) that the number of neighboring joints in the ANN adjacency matrix is based on the joints distribution in the pose. We note that after training, the model learns the threshold parameter  $T_{STB} = 0.052$  and  $T_{RHD} = 0.0448$  for the two datasets.

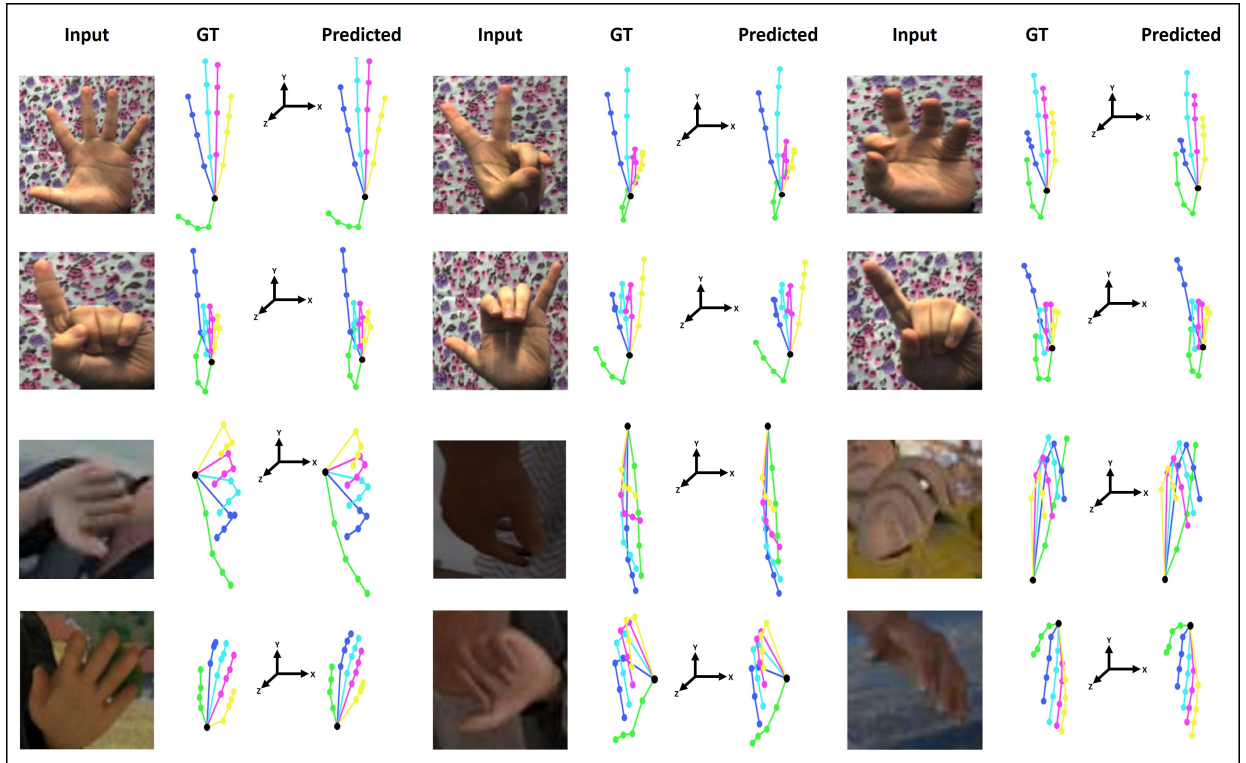


**Figure 5:** 3D hand pose estimation results on STB (first two rows) and RHD (last two rows) datasets. For each triplet, the left column represents the input RGB image, the middle column is the ground truth 3D joint skeleton and the right column is our corresponding prediction (This figure should be printed in color).

**Table 4**

Comparison with the state-of-the-art methods on RHD and STB datasets using Mean EPE [pixel].

Methods	RHD	STB
Zimmermann et al[17]	9.14	5
Iqbal et al [19]	3.57	-
Ours	<b>2.91</b>	<b>1.56</b>

#### 4.5. Qualitative results

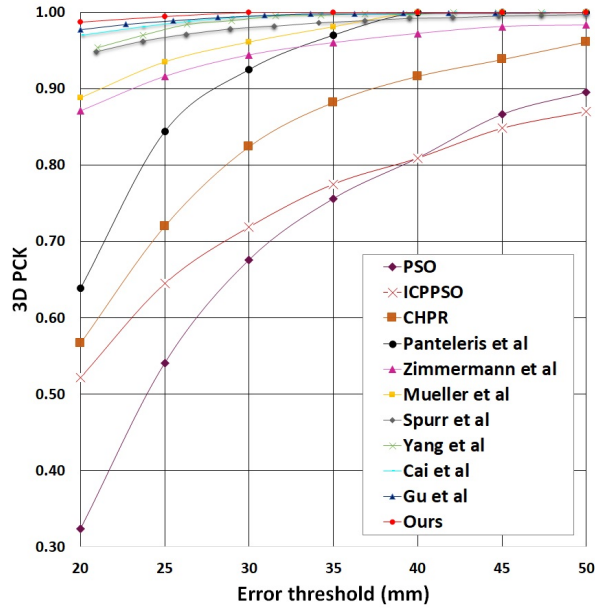
In addition to the quantitative validation, we show qualitative results of the proposed 2D/3D hand pose estimation method on STB and RHD datasets. Fig. 4 presents all the intermediate outputs, including the predicted poses and the learned per-pose adjacency matrices. We can see that the estimated 2D and 3D poses are very close to the ground truth, demonstrating that the proposed approach achieves accurate results for both 2D and 3D hand pose estimation. Furthermore, the 2D, 3D and ANN adjacency matrices reflect spatial relationships between the predicted joints that can be physically connected or disconnected in the hand skeletal.

Fig. 5 shows more qualitative results of the 3D hand pose estimation task on STB and RHD datasets. We can see that the estimated 3D poses are reliable even in case of self-occlusion and complex background textures. We also report more qualitative results for 2D hand pose estimation in Fig. A.1.

#### 4.6. Comparisons with state-of-the-art method

We report the quantitative results of the 2D hand pose estimation task with EPE (pixel), and we compare it against [17, 19]. We can see from Table. 4 that our approach achieves low errors in the two datasets and outperforms the state-of-the-art, proving that the 2D GCN-based regressor benefits from the learned per-pose constraint (2D relations matrix).

Since our main aim is to estimate the 3D hand pose, we compare the proposed method against several competitive



**Figure 6:** Comparison with the state-of-the-art methods [10, 13–17, 25, 29–31] on the STB dataset using 3D PCK (This figure should be printed in color).

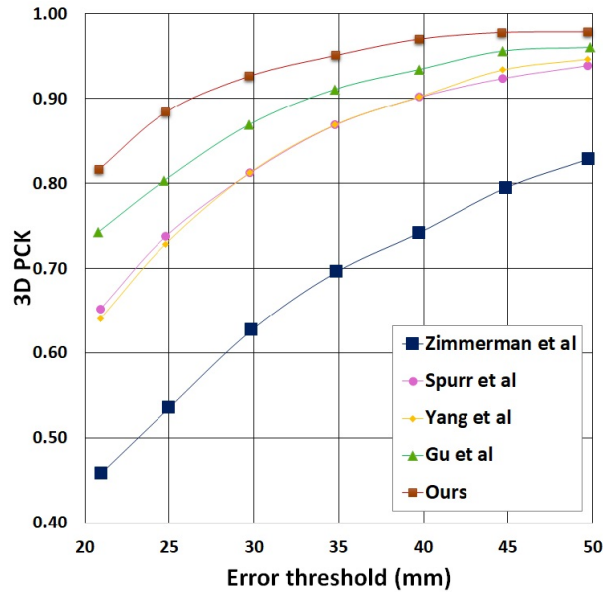


**Figure 7:** Comparison with the state-of-the-art methods [13–15, 17] on the RHD dataset using 3D PCK (This figure should be printed in color).

state-of-the-art on RHD and STB datasets with all the aforementioned metrics. For a fair comparison, we follow previous works preprocessing of the RHD dataset [17], and we validate the proposed method under the same evaluation conditions and standards and using the same data split. We use a range of 20 – 50 (mm) for the 3D PCK metric since it is a well-known standard criterion for RHD and STB dataset. Fig. 6 shows the 3D PCK results comparison on the STB dataset of our approach and several state-of-the-art methods [10, 13–17, 25, 29–31]. Our method outperforms [10, 13, 14, 16, 17, 29–31] and achieves competitive performances on the STB dataset to [15, 25]. To further evaluate our approach, we report the 3D PCK curves of the RHD dataset. Fig. 7 shows that our method outperforms the compared state-of-the-art methods [13–15, 17] on all the PCK thresholds.

**Table 5**

Comparison with the state-of-the-art methods on RHD and STB datasets using AUC.

Methods	RHD	STB
Zimmermann et al [17]	0.675	0.948
Mueller et al [10]	-	0.965
Spurr et al [13]	0.849	0.983
Cai et al [18]	0.887	0.994
Iqbal et al [19]	-	0.994
Yang et al [14]	0.849	0.991
Boukhayma et al [20]	-	0.994
Baek et al [34]	0.926	0.995
Ge et al [23]	0.920	0.998
Zhang et al [35]	0.901	0.995
Cai et al [25]	-	0.995
Guo et al [24]	0.933	0.998
Zhao et al [36]	0.872	0.987
Zhou et al [21]	0.856	0.898
Gu et al [15]	0.887	0.996
Ours	<b>0.939</b>	<b>0.998</b>

**Table 6**

Comparison with the state-of-the-art methods on RHD and STB datasets using Mean EPE [mm].

Methods	RHD	STB
Zimmermann et al [17]	30.42	8.68
Spurr et al [13]	19.73	8.56
Yang et al [14]	19.95	8.66
Gu et al [15]	17.11	7.27
Zhao et al [36]	-	8.18
Ours	<b>12.81</b>	<b>6.58</b>

We report the AUC of 3D PCK for a better understanding of the results. Table. 5 presents the results of the two datasets with additional state-of-the-art methods [18–21, 23, 24, 34–36]. We can see that the proposed approach has the highest score in the RHD dataset, improving the AUC value to 0.939. Also, there is a small improvement in the STB dataset (0.998). Note that the advantage of our approach appears in the RHD dataset that includes low-resolution images with complex backgrounds and poses. STB dataset is less challenging since it contains simple backgrounds with a restricted number of poses. Finally, Table. 6 lists the EPE metric comparison against five state-of-the-art methods [13–15, 17, 36]. We can see that the proposed method has superior performances providing 12.81 and 6.58 mean EPE on RHD and STB datasets, respectively. This is mainly due to the learned per-pose geometric constraint (adjacency matrix) and the ANN-based refinement module.

#### 4.7. Computation complexity

Although the proposed framework includes six modules, it is computationally efficient, where the running time on NVIDIA TITAN X GPU is 7ms. We can explain this by that the network consists of a lightweight feature extractor (ResNet10) and five GCN-based modules, which are significantly faster than convolutional neural networks [27]. While the classification modules (per-pose constraints) notably contributes to improving the 3D hand pose estimation accuracy, it necessitates only an additional 1ms per image, which does not speed down the inference time.

## 5. Conclusions

In this work, we propose an efficient GCN-based framework for 2D/3D hand pose estimation from a monocular RGB image. Our method addresses one of the key challenges of GCN by learning per-pose geometric constraints expressing local and global relationships between the hand joints. We obtain this information using a classification

step that exploits the spatial dependencies between the joint. We improve the predicted pose through a GCN-based refinement module that employs the proposed ANN algorithm to identify joint relationships based and we obtain more accurate 3D hand poses. Experimental results on realistic and synthetic datasets prove the competitiveness of our efficient approach compared to several state-of-the-art methods. In our future work, we plan to exploit temporal information to improve the overall model performance.

## Declaration of Competing Interest

The authors declare that they have no known competing financial interests or personal relationships that could have appeared to influence the work reported in this paper.

## Acknowledgement

This research did not receive any specific grant from funding agencies in the public, commercial, or not-for-profit sectors.

## References

- [1] Xuefeng Li, Yidan Zhou, Yi Sun, Xiangbo Lin, and Xiaohong Ma. A multi-branch hand pose estimation network with joint-wise feature extraction and fusion. *Signal Processing: Image Communication*, 81:115692, 2020.
- [2] Chengde Wan, Thomas Probst, Luc Van Gool, and Angela Yao. Crossing nets: Combining gans and vaes with a shared latent space for hand pose estimation. In *Proceedings of the IEEE Conference on Computer Vision and Pattern Recognition*, pages 680–689, 2017.
- [3] Shile Li and Dongheui Lee. Point-to-pose voting based hand pose estimation using residual permutation equivariant layer. In *Proceedings of the IEEE Conference on Computer Vision and Pattern Recognition*, pages 11927–11936, 2019.
- [4] Markus Oberweger and Vincent Lepetit. Deepprior++: Improving fast and accurate 3d hand pose estimation. In *Proceedings of the IEEE International Conference on Computer Vision Workshops*, pages 585–594, 2017.
- [5] Zheng Chen, Kuo Du, Yi Sun, Xiangbo Lin, and Xiaohong Ma. Hierarchical neural network for hand pose estimation. *Signal Processing: Image Communication*, page 115909, 2020.
- [6] Liuhaio Ge, Zhou Ren, and Junsong Yuan. Point-to-point regression pointnet for 3d hand pose estimation. In *Proceedings of the European conference on computer vision (ECCV)*, pages 475–491, 2018.
- [7] Gyeongsik Moon, Ju Yong Chang, and Kyoung Mu Lee. V2v-posenet: Voxel-to-voxel prediction network for accurate 3d hand and human pose estimation from a single depth map. In *Proceedings of the IEEE conference on computer vision and pattern Recognition*, pages 5079–5088, 2018.
- [8] Tomas Simon, Hanbyul Joo, Iain Matthews, and Yaser Sheikh. Hand keypoint detection in single images using multiview bootstrapping. In *Proceedings of the IEEE conference on Computer Vision and Pattern Recognition*, pages 1145–1153, 2017.
- [9] Robert Wang, Sylvain Paris, and Jovan Popović. 6d hands: markerless hand-tracking for computer aided design. In *Proceedings of the 24th annual ACM symposium on User interface software and technology*, pages 549–558, 2011.
- [10] Franziska Mueller, Florian Bernard, Oleksandr Sotnychenko, Dushyant Mehta, Srinath Sridhar, Dan Casas, and Christian Theobalt. Generated hands for real-time 3d hand tracking from monocular rgb. In *Proceedings of the IEEE Conference on Computer Vision and Pattern Recognition*, pages 49–59, 2018.
- [11] Francisco Gomez-Donoso, Sergio Orts-Escolano, and Miguel Cazorla. Large-scale multiview 3d hand pose dataset. *Image and Vision Computing*, 81:25–33, 2019.
- [12] Christian Zimmermann, Duygu Ceylan, Jimei Yang, Bryan Russell, Max Argus, and Thomas Brox. Freihand: A dataset for markerless capture of hand pose and shape from single rgb images. In *Proceedings of the IEEE International Conference on Computer Vision*, pages 813–822, 2019.
- [13] Adrian Spurr, Jie Song, Seonwook Park, and Otmar Hilliges. Cross-modal deep variational hand pose estimation. In *Proceedings of the IEEE Conference on Computer Vision and Pattern Recognition*, pages 89–98, 2018.
- [14] Linlin Yang and Angela Yao. Disentangling latent hands for image synthesis and pose estimation. In *Proceedings of the IEEE Conference on Computer Vision and Pattern Recognition*, pages 9877–9886, 2019.
- [15] Jiajun Gu, Zhiyong Wang, Wanli Ouyang, Jiafeng Li, Li Zhuo, et al. 3d hand pose estimation with disentangled cross-modal latent space. In *The IEEE Winter Conference on Applications of Computer Vision*, pages 391–400, 2020.
- [16] Paschalis Panteleris, Iason Oikonomidis, and Antonis Argyros. Using a single rgb frame for real time 3d hand pose estimation in the wild. In *2018 IEEE Winter Conference on Applications of Computer Vision (WACV)*, pages 436–445. IEEE, 2018.
- [17] Christian Zimmermann and Thomas Brox. Learning to estimate 3d hand pose from single rgb images. In *Proceedings of the IEEE international conference on computer vision*, pages 4903–4911, 2017.
- [18] Yujun Cai, Liuhaio Ge, Jianfei Cai, and Junsong Yuan. Weakly-supervised 3d hand pose estimation from monocular rgb images. In *Proceedings of the European Conference on Computer Vision (ECCV)*, pages 666–682, 2018.
- [19] Umar Iqbal, Pavlo Molchanov, Thomas Breuel Juergen Gall, and Jan Kautz. Hand pose estimation via latent 2.5 d heatmap regression. In *Proceedings of the European Conference on Computer Vision (ECCV)*, pages 118–134, 2018.
- [20] Adnane Boukhayma, Rodrigo de Bem, and Philip HS Torr. 3d hand shape and pose from images in the wild. In *Proceedings of the IEEE Conference on Computer Vision and Pattern Recognition*, pages 10843–10852, 2019.



- [21] Yuxiao Zhou, Marc Habermann, Weipeng Xu, Ikhsanul Habibie, Christian Theobalt, and Feng Xu. Monocular real-time hand shape and motion capture using multi-modal data. In *Proceedings of the IEEE/CVF Conference on Computer Vision and Pattern Recognition*, pages 5346–5355, 2020.
- [22] Thomas N. Kipf and Max Welling. Semi-supervised classification with graph convolutional networks. In *International Conference on Learning Representations (ICLR)*, 2017.
- [23] Liuhao Ge, Zhou Ren, Yuncheng Li, Zehao Xue, Yingying Wang, Jianfei Cai, and Junsong Yuan. 3d hand shape and pose estimation from a single rgb image. In *Proceedings of the IEEE conference on computer vision and pattern recognition*, pages 10833–10842, 2019.
- [24] Shaoliang Guo, Eric Rigall, Lin Qi, Xinghui Dong, Haiyan Li, and Junyu Dong. Graph-based cnns with self-supervised module for 3d hand pose estimation from monocular rgb. *IEEE Transactions on Circuits and Systems for Video Technology*, 2020.
- [25] Yujun Cai, Liuhao Ge, Jun Liu, Jianfei Cai, Tat-Jen Cham, Junsong Yuan, and Nadia Magnenat Thalmann. Exploiting spatial-temporal relationships for 3d pose estimation via graph convolutional networks. In *Proceedings of the IEEE International Conference on Computer Vision*, pages 2272–2281, 2019.
- [26] Long Zhao, Xi Peng, Yu Tian, Mubbasir Kapadia, and Dimitris N Metaxas. Semantic graph convolutional networks for 3d human pose regression. In *Proceedings of the IEEE Conference on Computer Vision and Pattern Recognition*, pages 3425–3435, 2019.
- [27] Bardia Doosti, Shujon Naha, Majid Mirbagheri, and David J Crandall. Hope-net: A graph-based model for hand-object pose estimation. In *Proceedings of the IEEE/CVF Conference on Computer Vision and Pattern Recognition*, pages 6608–6617, 2020.
- [28] Kaiming He, Xiangyu Zhang, Shaoqing Ren, and Jian Sun. Deep residual learning for image recognition. In *Proceedings of the IEEE conference on computer vision and pattern recognition*, pages 770–778, 2016.
- [29] Jiawei Zhang, Jianbo Jiao, Mingliang Chen, Liangqiong Qu, Xiaobin Xu, and Qingxiong Yang. 3d hand pose tracking and estimation using stereo matching. *arXiv preprint arXiv:1610.07214*, 2016.
- [30] Chen Qian, Xiao Sun, Yichen Wei, Xiaoou Tang, and Jian Sun. Realtime and robust hand tracking from depth. In *Proceedings of the IEEE conference on computer vision and pattern recognition*, pages 1106–1113, 2014.
- [31] Iason Oikonomidis, Nikolaos Kyriazis, and Antonis A Argyros. Efficient model-based 3d tracking of hand articulations using kinect. In *Bmvc*, volume 1, page 3, 2011.
- [32] Ian Goodfellow, Jean Pouget-Abadie, Mehdi Mirza, Bing Xu, David Warde-Farley, Sherjil Ozair, Aaron Courville, and Yoshua Bengio. Generative adversarial nets. In *Advances in neural information processing systems*, pages 2672–2680, 2014.
- [33] Diederik P. Kingma and Max Welling. Auto-encoding variational bayes. 2014.
- [34] Seungryul Baek, Kwang In Kim, and Tae-Kyun Kim. Pushing the envelope for rgb-based dense 3d hand pose estimation via neural rendering. In *Proceedings of the IEEE Conference on Computer Vision and Pattern Recognition*, pages 1067–1076, 2019.
- [35] Xiong Zhang, Qiang Li, Hong Mo, Wenbo Zhang, and Wen Zheng. End-to-end hand mesh recovery from a monocular rgb image. In *Proceedings of the IEEE International Conference on Computer Vision*, pages 2354–2364, 2019.
- [36] Long Zhao, Xi Peng, Yuxiao Chen, Mubbasir Kapadia, and Dimitris N Metaxas. Knowledge as priors: Cross-modal knowledge generalization for datasets without superior knowledge. In *Proceedings of the IEEE/CVF Conference on Computer Vision and Pattern Recognition*, pages 6528–6537, 2020.
- [37] Julieta Martinez, Rayat Hossain, Javier Romero, and James J Little. A simple yet effective baseline for 3d human pose estimation. In *Proceedings of the IEEE International Conference on Computer Vision*, pages 2640–2649, 2017.
- [38] Haoshu Fang, Yuanlu Xu, Wenguan Wang, Xiaobai Liu, and Song-Chun Zhu. Learning pose grammar to encode human body configuration for 3d pose estimation. *AAAI*, 2018.
- [39] Zhongdao Wang, Liang Zheng, Yali Li, and Shengjin Wang. Linkage based face clustering via graph convolution network. In *Proceedings of the IEEE Conference on Computer Vision and Pattern Recognition*, pages 1117–1125, 2019.
- [40] Chao Qi, Jianming Zhang, Hongjie Jia, Qirong Mao, Liangjun Wang, and Heping Song. Deep face clustering using residual graph convolutional network. *Knowledge-Based Systems*, 211:106561.
- [41] Xiaojuan Qi, Renjie Liao, Jiaya Jia, Sanja Fidler, and Raquel Urtasun. 3d graph neural networks for rgbd semantic segmentation. In *Proceedings of the IEEE International Conference on Computer Vision*, pages 5199–5208, 2017.
- [42] Adam Paszke, Sam Gross, Soumith Chintala, Gregory Chanan, Edward Yang, Zachary DeVito, Zeming Lin, Alban Desmaison, Luca Antiga, and Adam Lerer. Automatic differentiation in pytorch. 2017.
- [43] Xavier Glorot and Yoshua Bengio. Understanding the difficulty of training deep feedforward neural networks. In *Proceedings of the thirteenth international conference on artificial intelligence and statistics*, pages 249–256, 2010.
- [44] Matthew D Zeiler. Adadelta: an adaptive learning rate method. *arXiv preprint arXiv:1212.5701*, 2012.
- [45] Diederik P Kingma and Jimmy Ba. Adam: A method for stochastic optimization. *International Conference on Learning Representations ICLR*, 2015.
- [46] Jiawei Zhang, Jianbo Jiao, Mingliang Chen, Liangqiong Qu, Xiaobin Xu, and Qingxiong Yang. A hand pose tracking benchmark from stereo matching. In *2017 IEEE International Conference on Image Processing (ICIP)*, pages 982–986. IEEE, 2017.

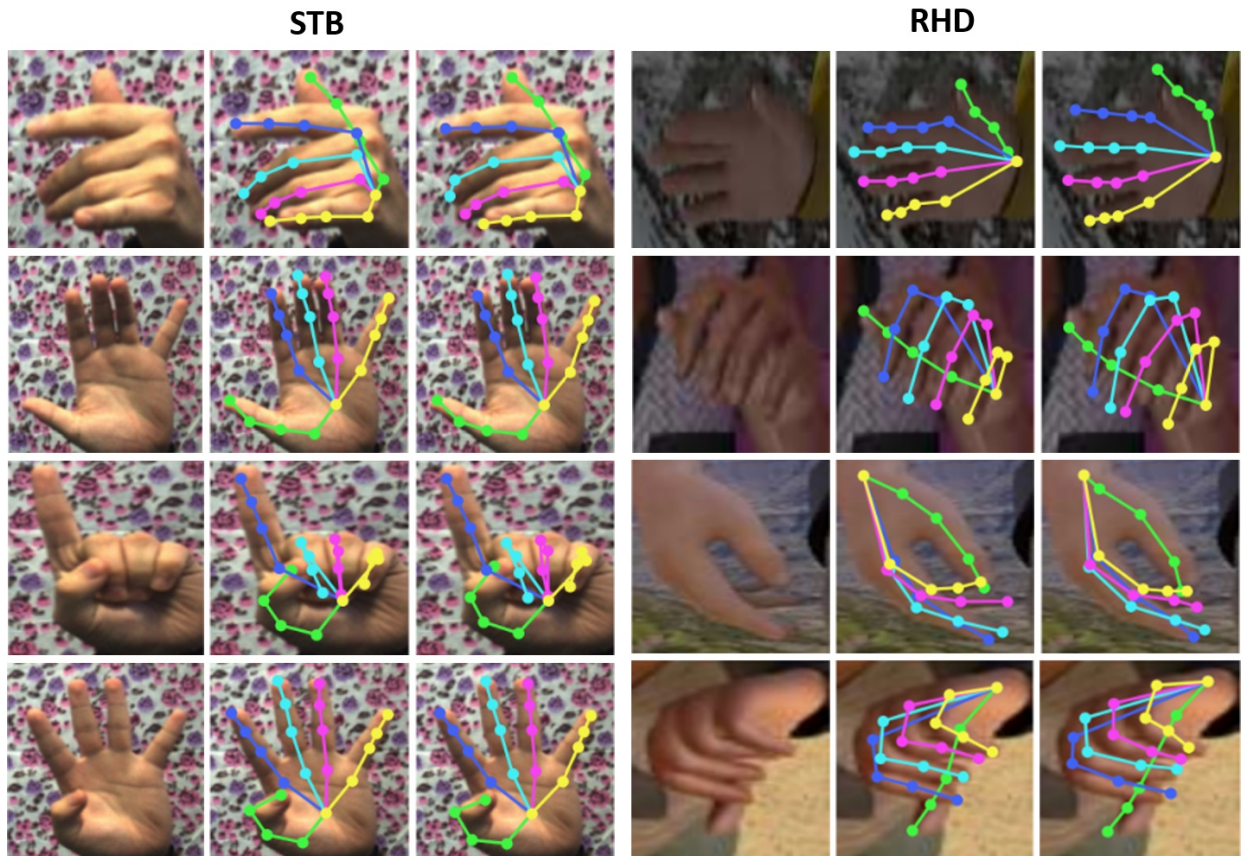


**Figure A.1:** 2D hand pose estimation results on STB and RHD datasets. For each triplet, the left column represents the input RGB image, the middle column is the ground truth 3D joint skeleton and the right column is our corresponding prediction (This figure should be printed in color).

## Supplementary material

### A. 2D qualitative results

We provide qualitative results for 2D hand pose estimation in Fig. A.1. This task also has several applications, such as sign language and gesture recognition. We can see that the proposed approach produces accurate 2D poses on STB and RHD datasets.

### B. Ground truth of 2D/3D joints classification task

In this section, we explain the creation of the ground truth 2D/3D classes. The function *CreateClasses2D* in Algorithm. 3 creates an array of size 21, where each value represent the class of a specific 2D joint. The inputs are the  $(x, y)$  coordinates of the 2D keypoints, the number of splits and the image size (the width and height must be equal). Following, we explain the algorithm by specifying the line number and a brief description of its functionality. Note that our algorithms follow a Pythonic pseudo-code style.

- *Line 2* calculates the size of each block.
- *Line 6 to 8* initializes the *parts* array, which represents the beginning and the end of the blocks in the  $x/y$  axis, e.g.: if the number of splits is 4,  $parts = [0, 64, 128, 192, 256]$ , where  $C_0 \in [0, 64]$ ,  $C_1 \in [64, 128]$ , etc.
- *Line 9 to 14*: for each block (class), *data* contains the  $x$  and  $y$  intervals, where the joints are located, e.g.:  $data[0] = [0, 32, 64, 128]$  if  $joint_0$  is in the interval  $[0, 32]/[64, 128]$  in the  $x/y$  axis, respectively.

A hybrid classification-regression approach for 3D hand pose estimation using graph convolutional networks

- In *Line 15 to 17*, *classes* is a dictionary, where the key is the joint number and the value is a zero vector. To fill in the latter, we iterate over all the (*key, value*) pairs in *data* to evaluate the boolean expression in *Line 19*. The latter creates a boolean vector of size 21 such that each value is *True/False* if the joint is inside/outside the the *x/y* intervals.
- *Line 20 to 24*: we get the one-hot vector of each joint by assigning the position of the correct class in the zero-vector to 1.
- From *Line 27 to 30*, *output* is an array of size 21, where we get the class of each joint using the *Argmax* function on the one-hot vectors.

We follow the same analogy in Algorithm. 4 to create the ground truth classes of each joint in the 3D space.

---

**Algorithm 3:** Creation of the 2D ground truth classes of each joint in a cropped hand.

---

```

1 function CreateClasses2D (2D, splits, size);
   Input : (x, y) points, splits number and image size
   Output: An array containing the class of each 2D joint
2 block ← int(size/splits);
3 parts, data, output ← [];
4 classes ← {};
5 k ← 0;
6 for i in range(0, size + block, block) do
7   | parts[i] ← i;
8 end
9 for j=0:splits do
10  | for i=0:splits do
11  |   | data[k] ← [parts[j], parts[j + 1], parts[i], parts[i + 1]];
12  |   | k ← k + 1;
13  | end
14 end
15 for i=0:21 do
16  | classes[i] ← [0, ..., 0];
17 end
18 for key, (ax, bx, ay, by) in data.items() do
19  | r ← (ax ≤ 2D[:, 0]) & (bx ≥ 2D[:, 0]) & (ay ≤ 2D[:, 1]) & (by ≥ 2D[:, 1]);
20  | for i=0:21 do
21  |   | if r[i] = True then
22  |   |   | classes[i][key] ← 1;
23  |   | end
24  | end
25 end
26 i ← 0;
27 for key, val in classes.items() do
28  | output[i] ← argmax(val);
29  | i ← i + 1;
30 end
31 return output;

```

---

**Algorithm 4:** Creation of the 3D ground truth classes of each joint in a cropped hand.

---

```

1 function Create3DClasses (3D, splits);
   Input : (x, y, z) points and splits number
   Output: An array containing the class of each 3D joint
2 startx_3d, starty_3d, startz_3d ← min(3D[:, 0]), min(3D[:, 1]), min(3D[:, 2]);
3 endx_3d, endy_3d, endz_3d ← max(3D[:, 0]), max(3D[:, 1]), max(3D[:, 2]);
4 intervalx_3d ← endx_3d - startx_3d;
5 intervaly_3d ← endy_3d - starty_3d;
6 intervalz_3d ← endz_3d - startz_3d;
7 stepx ← float(intervalx_3d/splits);
8 stepy ← float(intervaly_3d/splits);
9 stepz ← float(intervalz_3d/splits);
10 partsx, partsy, partsz ← [];
11 data, output ← [];
12 classes ← {};
13 k ← 0;
14 rangex = arange(startx_3d, endx_3d + stepx, stepx);
15 rangey = arange(starty_3d, endy_3d + stepy, stepy);
16 rangez = arange(startz_3d, endz_3d + stepz, stepz);
17 for i, j, k in rangex, rangey, rangez do
18 | partsx[i] ← i, partsy[j] ← j, partsz[k] ← k;
19 end
20 for i=0:21 do
21 | classes[i] ← [0, ..., 0];
22 end
23 for j=0:n_splits do
24 | for i=0:n_splits do
25 | | for p=0:n_splits do
26 | | | data[k] ← [partsx[j], partsx[j + 1], partsy[i], partsy[i + 1], partsz[p], partsz[p + 1]];
27 | | | k ← k + 1;
28 | | | end
29 | | end
30 end
31 for key, (ax, bx, ay, by, az, bz) in data.items() do
32 | r ← (ax ≤ 3D[:, 0]) & (bx ≥ 3D[:, 0]) & (ay ≤ 3D[:, 1]) & (by ≥ 3D[:, 1]) & (az ≤ 3D[:, 2])
   & (bz ≥ 3D[:, 2]);
33 | for i=0:21 do
34 | | if r[i] = True then
35 | | | classes[i][key] ← 1;
36 | | | end
37 | | end
38 end
39 i ← 0;
40 for key, val in classes.items() do
41 | output[i] ← argmax(val);
42 | i ← i + 1;
43 end
44 return output;

```

---